Waste Management 171 (2023) 452–462

Contents lists available at ScienceDirect

Waste Management

journal homepage: www.elsevier.com/locate/wasman

Research Paper

New insights into the production, characterization and potential uses of vineyard pruning waste biochars

Eliana Cárdenas-Aguiar [a,b,*], Gabriel Gascó [a], Marcos Lado [b], Ana Méndez [c], Jorge Paz-Ferreiro [d], Antonio Paz-González [b]

[a] Department of Agricultural Production, Universidad Politécnica de Madrid, Ciudad Universitaria, 28040 Madrid, Spain
[b] Centro Interdisciplinar de Química e Bioloxía- CICA, As Carballeiras, s/n Campus de Elviña, Universidade da Coruña, 15008 Coruña, Spain
[c] Department of Geological and Mining Engineering, Universidad Politécnica de Madrid, 28040 Madrid, Spain
[d] School of Engineering, RMIT University, Melbourne, VIC 3000, Australia

ARTICLE INFO

Keywords:
Vineyard pruning
Biochars
Pyrolysis parameters

ABSTRACT

Vineyard pruning waste (VP) can be converted into a useful char using pyrolysis as part of a valorization strategy. This study analyzed the effect of temperature (300 and 600 °C) and residence time (1 and 3 h) on an ample number of properties of VP derived biochars, including potential negative environmental impacts. The results showed a clear influence of temperature on biochar's properties and a weaker effect of residence time. Increasing temperature raised soil pH, electrical conductivity (EC), ash and C contents, aromaticity, specific surface area, solid density, mesoporosity and partial graphitization. However, higher pyrolysis temperature reduced O/C and N/C ratios, total N, P and Mg, and polycyclic aromatic hydrocarbons (PAHs). Particularly, the concentration of water extractable organic carbon (WEOC) decreased dramatically with pyrolysis temperature. Moreover, the WEOC fraction of biochars pyrolyzed at 300 °C exhibited a larger aromaticity than those pyrolyzed at 600 °C. Prolonged residence time increased ash content and fixed carbon (FC) and decreased H/C and O/C ratios; however, most frequently this parameter affected biochar properties following opposite trends for the two pyrolysis temperatures. Hydrophysical properties were adequate to consider VP derived biochars as growing media component. PAH concentration was much lower than thresholds following international standards. The germination index increased with temperature and decreased with residence time, so that phytotoxicity was observed in VP and in biochars pyrolyzed for 3 h. Our research demonstrates that, besides temperature, residence time can be useful to modulate the properties of biochars and that prolonged time effect is temperature-dependent.

1. Introduction

Biochar is a carbonaceous material obtained from the thermochemical conversion of biomass. A variety of feedstocks have been used for pyrolysis, including wood-based products, organic and industrial wastes, among others (Liu et al., 2020). Pyrolysis process parameters and feedstocks characteristics influence biochar properties. Broadly, biochars can be divided in two groups, those derived from woody biomass (lignocellulosic materials) and those produced from non-woody biomass. The first one, for example forest residues, possesses a low ash content, leading to stable biochars which can be applied for soil carbon sequestration (Feng et al., 2020). Meanwhile, non-woody biochars have high ash content, for example animal manure, urban and industrial solid residues and agricultural waste, and can contribute to an increase in soil fertility (Tomczyk et al., 2020).

Pyrolysis temperature, residence time, heating rate and feedstock are crucial to understand the characteristics of the resulted biochars (Devi and Saroha, 2015; Wang et al., 2020). Many studies have been devoted to the effects of feedstock and temperature, on biochar properties. Biochars consistently have been prepared in the range from 300 to 900 °C and mostly between 300 and 600 °C (Al-Wabel et al., 2013; Banik et al., 2018; Suliman et al., 2016: Gascó et al., 2018; Cárdenas Aguiar et al., 2019., Tomczyk et al., 2020; Greco et al., 2021). Temperature rise produces biochars with a higher degree of carbonization and aromaticity. This results in increasing pH, electrical conductivity ash content; surface area and porosity and decreasing water extractable organic

* Corresponding author at: Universidad Politécnica de Madrid, Spain and Universidade da Coruña.
E-mail addresses: eliana.cardenas@col.udc.es, eliana.cardenas@upm.es (E. Cárdenas-Aguiar), gabriel.gasco@upm.es (G. Gascó), marcos.lado@udc.es (M. Lado), anamaria.mendez@upm.es (A. Méndez), jorge.paz-ferreiro@rmit.edu.au (J. Paz-Ferreiro), antonio.paz.gonzalez@udc.es (A. Paz-González).

https://doi.org/10.1016/j.wasman.2023.09.032
Received 13 July 2023; Received in revised form 9 September 2023; Accepted 22 September 2023
Available online 4 October 2023

content (Gascó et al., 2018; Cárdenas-Aguiar et al., 2019; Tomczyk et al., 2020; Wang et al., 2020).

Residence time has been less frequently considered in the study of biochar's properties. However, a wide range of pyrolysis durations, from 30 min to 5 h, has been studied (Benavente et al., 2018; Wang et al., 2020). Similar but weaker effects as those for temperature have been reported for prolonged residence time (Wang et al., 2020). This influence was evident at temperatures below 500 °C. For example, extending residence time from 30 min to 1 h led to a biochar with higher CEC and P_{Olsen} (Benavente et al., 2018).

Biochar addition to soil produces changes in soil properties, particularly biological and chemical properties (Lehmann et al., 2011). However, the influence of biochar addition in soil physical and hydraulic properties has been less studied (Blanco-Canqui, 2017) and is mostly governed by soil type, biochar feedstock and dosage. In general, biochar decreases soil bulk density and increases aggregate stability, total porosity, available water holding capacity and saturated hydraulic conductivity (Razzaghi et al., 2020). The decrease in soil bulk density has been widely reported in all types of soils textures (Głąb et al., 2016; Obia et al., 2016).

Additionally, hydrophysical properties of biochars play an important role if biochar is used as growing media component. A previous work stated that the mixing of peat with pruning waste derived biochars prepared at 300 °C and 500 °C can increase the bulk density of the substrate (Nieto et al., 2016). However, biochars prepared at low temperatures did not show a significant effect in the soil aeration capacity.

The wine industry generates large amounts of waste that are generally burnt in the field (Florindo et al., 2022) or directly applied to the soil but no added value is considered in this process. For that reason, it is important to study some alternatives to manage the large amount of VP wastes generated. Vineyard pruning waste derived biochars can be suitable approach not only as a valorization strategy but also as growing media component or soil amendment.

The use of vineyard pruning waste derived biochars can provoke unintended consequences but in other to avoid these effects, it is necessary to determine concentrations and signatures of Polycyclic Aromatic Hydrocarbons (PAHs) yielded by biochars produced under different pyrolysis conditions (Bucheli et al., 2019). Several PAHs are classified as priority pollutants and are strictly regulated by agencies, including US EPA and European Commission. Therefore, concentrations of PAHs in biochars are of concern because of their long residence time and their potential impact on human health and environmental conservation. In addition, seed tests (Zucconi et al., 1985) have been commonly used, not only to assess seed quality but also to appraise potential phytotoxicity of soil amendments like biochars, thus allowing an evaluation of sustainability. Benavente el al., (2018) reported that biochar prepared at 300 °C resulted in lower germination index values, while the biochar prepared at 500 °C produced a phytostimulant effect.

Biochar from pruning vineyard residues has been previously characterized (Egri et al., 2022) using proximate and elemental analysis together with several additional techniques. However, there is still room for improving knowledge about their structure and properties. For example, to our best knowledge, until now fluorescence spectroscopy has not been used to study pruning waste biochar. Following the literature review and previous work (Gascó et al., 2018; Cárdenas-Aguiar, 2019) four different biochars were prepared at temperatures of 300 and 600 °C and residence times of 1 h and 3 h. In addition to proximate and elemental analysis, and analysis of general physical and chemical properties we employed a wide series of more advanced technique to characterized the biochars produced from pruning waste, including thermogravimetric analyses, N_2 isotherm, Hg porosimetry, X-ray diffraction (XRD), scanning electron microscopy (SEM), infrared spectroscopy (FTIR), water extractable organic carbon (WEOC) and fluorescence spectroscopy (EEM); the joint use of this methods for characterization of pruning vineyard waste is also novel.

The main objective of the present work is to study the influence of pyrolysis parameters, temperature and residence time, in the chemical and physical properties of vineyard pruning waste derived biochars and evaluate their potential implications as soil amendment or growing media component. Additionally, PAHs content and phytotoxicity test was performed in order to prevent potential negative environmental impacts brought about by the use of vineyard pruning waste derived biochars.

2. Materials and methods

2.1. Feedstock selection and biochar fabrication

The vineyard pruning waste (VP) were collected from a vineyard located in the municipality of Paderne, A Coruña, Norwest of Spain. VP samples were air dried at 60 °C during 48 h and then cut into small pieces (<2 cm). Biochars were produced from pyrolysis of VP in a 12-PR/400 series 8B furnace (Hobersal, Spain) at 300 and 600 °C, using a heating rate of 3 °C min^{-1} and two residence times (1 h and 3 h), referred to as BVP300-1 h, BVP300-3 h, BVP600-1 h and BVP600-3 h.

2.2. Characterization of biochars

2.2.1. Chemical properties

The four biochars were passed through a 2 mm sieve prior to characterization. The chemical properties were determined as follows: (i) pH and electrical conductivity (EC) were measured in an aqueous suspensions of 1:250 (m/v) sample: water, previously stirred for 1 h in a Rotabit and Boxcult 230 V stirrer (JP Selecta, Spain), with a micro pH 2000 (Crison, Spain) and a micro cm 2201 conductivimeter (Crison, Spain); (ii) cation exchange capacity (CEC) was measured in a cohex extractant solution (0.5:25 m/v) in a Analyst 400 Atomic Absorption Spectrophotometer (PerkinElmer, United States) (Ciesielski and Sterckeman, 1997); and (iii) the easily oxidized organic carbon (Coxi) was calculated using the method by Walkley Black (Nelson and Sommers, 1996).

A DBS-30 halogen moisture analyzer (Kern & Sohn GmbH, Germany) was used to determine the moisture content at 105 °C until constant sample weight. The volatile matter (VM) content was calculate according to weight lost after placed covered quartz crucibles at to 900 °C for 7 min in a CR-48 furnace (Hobersal, Spain). The ash content was determined in a AAF 11/18 furnace (Carbolite Gero, United Kingdom) with covered alumina crucibles heated at 900 °C for 12 h. The fixed carbon (FC) was calculated as follows: FC = 100% − (%VM+ %Ash) (Igalavithana et al., 2017).

The content of carbon (C), hydrogen (H), nitrogen (N) and sulphur (S) were measured in a FlashEA1112 elemental analyzer (Thermo-Finnigan, United States). Oxygen (O) content was calculated by difference as O (%) = 100− (C + H + N + S + Ash).

Total P, K, Ca, Mg, Na, Fe, Mn, Cu and Zn contents were measured after the digestion of samples with 3:1 (v/v) of concentrated HCl and HNO_3 according to the USEPA 3051a method (U.S. EPA, 2007) using inductively coupled plasma mass spectrometry (ICP-MS) in an ELEMENT XR (Thermo-Finnigan, United States) equipment. The content of P_2O_5, K_2O, CaO, MgO, Fe_2O_3, MnO, CuO, ZnO, SiO_2 and SO_3S_4 were measured in the ash of biochars with a PIONEER (Bruker AXS GmbH, Germany) wavelength dispersive X-ray fluorescence spectrometer (WDXRF) using an X-ray fluorescence (XRF).

For the infrared spectroscopy 1 μg of sample was weighted and ground with 200 μg of KBr (KBr - FTIR grade-Panreac) in order to form pellets with 2 MPa of applied pressure with a Specac Mini Pellet Press for each sample and replicate. Then the samples were analysed with a Thermo Scientific is10 FTIR spectrometer (Thermo-Fisher Scientific, United States) in transmission mode with a wavenumber ranged between: 400 and 4000 cm^{-1} and a resolution of 1 cm^{-1}. After collection, a Savitzky-Golay filter was applied and scatter effects were corrected with an Extended Multiplicative Scatter Correction (EMSC) method (Afseth

and Kohler, 2012) using R and the package EMSC (Liland, 2021). The final spectrum for VP and biochars were the average of 6 corrected spectra (3 pellets × 2 spectra from each pellet).

The water extractable organic carbon (WEOC) was measured with a Formacs HT analyzer (Skalar, United States) in aqueous extracts with a sample:water ratio 1:4 (m/v), previously stirred for 1 h and posterior filtration at 2.5 μm. The UV–Vis absorbance spectra and fluorescence EEMs were measured in WEOC extracts in a 1-cm quartz cuvette in the 200–1000 nm range in 2 nm increments using a Zuzi UV–Vis 4418 spectrophotometer (Auxilab, Spain). Extracts were diluted when the absorbance of the samples was above 1.5, to ensure that the measurements were done in the range of concentrations where Lambert-Beer law applies (Kothawala et al., 2013). A commonly index used to characterize WEOC, was determined with the specific UV–Vis absorbance at 254 nm ($SUVA_{254}$ index), divided by the optical path (1 cm) and multiplied by 100.

Total fluorescence was determined as the sum of all emission intensities in the EEMs. Fluorescence EEMs were measured in WEOC extracts or their dilutions using a FluoroMax® – 4P spectrofluorometer (Horiba, Japan). The excitation and emission wavelengths (λ) were between 220 and 520 nm, and 224 and 700 nm respectively in 4 nm increments. The S/R ratio was used to account for differences in the intensity of the excitation light, meaning that for each excitation wavelength, emission intensities (S) were corrected against those measured in a reference detector (R). One of the correction correspond to the removal of Rayleigh scattering, the second one included the inner filter effect correction (Lakowicz, 2013), and the third the subtraction of EEMs of blank samples (Borisover et al., 2009). The EEMs were stated in Raman units with a water Raman peak intensity at ex/em 300/397 nm (Holbrook et al., 2006).

2.2.2. Physical properties

Mercury intrusion porosimetry was determined with a Porosimeter AutoPore IV Mercury (Micromeritics, United States). The BET surface area (S_{BET}) and pore size distributions were determined from N_2 adsorption isotherms by a TriStar II Plus Version 3.00 analyzer (Micromeritics, United States). The micropores were defined to be <2 nm of diameter, mesopores between 2 and 50 nm and macropores >50 nm (Wong and Ogbonnaya, 2021). For the micropores the data were obtained with N_2 isotherms and for meso and macropores with Hg porsimetry.

The hydrophysical properties of the biochars were assessed for the biochars sieved at 4 mm, using a container with known weight (W_0), 100 mL volume capacity, and a drainage hole sealed at the bottom. The container was filled with each dry sample (Wd) and then distillated water was added slowly in the surface until complete saturation. The container was placed over a sealed plastic tray. The seal was removed from the container drain hole, in order to allow all the free water to drain out of. Subsequently, the entire content of saturated biochars was weighted (Ww), resulting in the water holding capacity (WHC) determination by the following formula: $WHC\ (\%) = [(Wd-(Ww-W_0))/(100\ mL)] \times 100$.

The total porosity (TP) was calculated with the bulk density (BD) and solid density (SD) of the samples by TP (%) = (1-(BD/SD))*100. Then the aeration capacity (AC) was determined by AC (%)= %TP-%WHC (Méndez et al., 2015). The SD was measured with an Accupyc 1340 helium pycnometer (Micromeritics, United States) and BD was assessed with a known volume container filled with the sample and weighted.

The XRD (X-ray diffraction) analysis were conducted by a JSM 6400 microscope (JEOL, United States) and D4 Endeavor diffractometer (Bruker AXS GmbH, Germany) respectively (Igalavithana et al., 2017). Scanning electron micrographs (SEM) of the VP and the BVP300-1 h and BVP600-1 h biochars were taken using the JSM 6400 (JEOL, USAS) Scanning Electron Microscope (SEM). The instrument was operated at with an acceleration voltage of 25 kV (Chia et al., 2012; Suliman et al., 2016).

2.2.3. Thermogravimetric analysis (TGA)

The TGA instrument was operated with a flux of 60 mL min^{-1} and N_2 atmosphere and each material was heated up to 1000 °C using a STA 449F3 analyzer (Netzsch, Germany) then the TGA and the differential thermal analyzer (DTA) graphics were obtained. The samples weight for TGA varied between 20 and 30 mg and placed in alumina crucibles DSC/TG pan Al_2O_3 and with a heating rate of 10 °C min^{-1}.

2.2.4. Environmental implications

PAHs analysis and germination tests were performed in order to evaluate the environmental risk of use VP waste derived biochars. Prior to PAHs analysis, biochars were dried, grinded (0.2 mm), homogenized and stored at a dry place. Method for PAHs determination in biochar generally include three steps: extraction with solvents, cleaning up the extracts, and quantitative analysis (Wang et al., 2017). Briefly, a microwave assisted extraction procedure was used, as this technique heats the whole sample fast and simultaneously, thereby reducing extraction time and solvent usage. Also, this method provides selective interaction with polar molecules, which greatly enhances the extraction efficiency of PAHs. A mixture acetone/hexanol 1:1 was used as extractant. Cleanup of the biochar extracts was performed by means of liquid–solid chromatography, using an alumina column and hexane elution. Quantitative determination was carried out by GC/MS, i.e. gas chromatography equipped with a fused silica capillary column for separation and a mass spectrometer coupled with triple quadrupole (Agilent 7010B); deuterated compounds were used as the internal standards for quantification.

The 16 PAHs listed as priority pollutants by the United States Environmental Protection Agency from here on referred to as “the 16 EPA PAHs” were analyzed. In addition, according to the number of aromatic rings the PAHs were classified as: light, medium and heavy (Greco et al., 2021).

Germination test was performed in order to assess the phytotoxicity of the materials. According to this test (Zucconi et al., 1985) the percentage of germination (%G) and the length of the germinated seeds (L) were used to calculated the germination index (GI). GI values < 50% were classified as highly phytotoxic; GI between 50 and 80% as moderately phytotoxic, GI > 80% as non-phytotoxic and GI > 100% as phytostimulant. The germination test was performed using *Lepidium sativum* as seed.

2.2.5. Statistical analysis

The differences of means for the three replicates of each sample were evaluated by the analysis of variance (ANOVA) and the Duncan’s multiple range test ($p < 0.05$) with the Statgraphics Centurion XVI.I. software.

3. Results and discussion

3.1. Chemical properties

Table 1 summarizes the chemical properties of VP and four derived biochars (BVP300-1 h, BVP300-3 h, BVP600-1 h and BVP600-3 h). The pH increased after pyrolysis, which is in agreement with previous research, due to the separation of alkali salts from organic materials and the increase in carbonate content (Mandal et al., 2018). Additionally, the loss of carboxylic groups with pyrolysis temperature can contribute to this. In general, the pH values were high and positively correlated not only with the ash content (Pearsoń’s $r = 0.94$, $p < 0.01$) but also with the sum of total K and Na content, i.e. alkali metals (Pearsoń’s $r = 0.91$, $p < 0.01$). The EC also increased with pyrolysis temperature and residence time. These results suggest some salt formation and concentration in ashes during pyrolysis, due to the breakdown of some organic structures increasing salt solubilization (Al-Wabel et al., 2013).

The CEC values showed an evident diminution for biochars compared to the feedstock, without statistically significant differences between the four biochars. The results can be related to the loss of O on

Table 1
Chemical properties of VP and vineyard pruning waste derived biochars samples (BVP300-1 h, BVP300-3 h, BVP600-1 h and BVP600-3 h). Means with the same letter are not significantly different ($p > 0.05$) using Duncan test for each variable independently.

Properties	VP	BVP300-1 h	BVP300-3 h	BVP600-1 h	BVP600-3 h
pH	6.77 ± 0.06a	8.55 ± 0.12b	8.88 ± 0.11c	9.93 ± 0.07d	9.76 ± 0.11d
EC (μS cm^{-1})	79.03 ± 1.75a	106.75 ± 2.9b	104.15 ± 0.78b	121.23 ± 0.76c	135.05 ± 0.35d
CEC (cmolc Kg^{-1})	93.51 ± 0.02b	9.89 ± 3.93a	16.38 ± 0.98a	22.89 ± 12.06a	21.7 ± 1.84a
C_{oxi} (%)	38.14 ± 1.19d	15.05 ± 0.27c	10 ± 0.71b	2.48 ± 0.16a	2.85 ± 0.26a
Moisture (%)	9.84	6.91	7.36	7.72	8.47
VM (%)	75.02	36.7	34	12	9.3
Ash (%)	2.18	3.1	3.58	4.71	5.19
FC (%)	22.80	60.2	62.42	83.29	85.51
N (%)	0.63	1.22	1.24	1.05	0.98
C (%)	40.61	67.04	67.68	77.17	76.94
H (%)	5.71	4.26	3.99	1.77	1.44
S (%)	0.15	0.03	0.02	0.02	0.02
O (%)	50.72	24.39	23.51	15.31	15.44
H/C	1.69	0.76	0.71	0.27	0.22
O/C	0.94	0.27	0.26	0.15	0.15
(O + N)/C	0.95	0.29	0.28	0.16	0.16

Table 2
Total element content of VP and vineyard pruning waste derived biochars (BVP300-1 h, BVP300-3 h, BVP600-1 h and BVP600-3 h). Means with the same letter are not significantly different ($p > 0.05$) using Duncan test for each variable independently.

Properties	VP	BVP300-1 h	BVP300-3 h	BVP600-1 h	BVP600-3 h
Total element content (g kg^{-1})					
P	0.93 ± 0.05a	2.24 ± 0.11e	2.11 ± 0.05d	1.63 ± 0.05c	1.35 ± 0.05b
K	5.96 ± 0.01a	14.37 ± 1.04b	13.99 ± 0.27b	15.82 ± 0.86c	13.67 ± 0.8b
Ca	5.36 ± 0.33c	4.67 ± 0.17b	5.25 ± 0.11c	4.21 ± 0.14a	5.16 ± 0.28c
Na	0.35 ± 0.05a	0.45 ± 0.04b	0.44 ± 0.04b	0.43 ± 0.01b	0.57 ± 0.05c
Mg	1.55 ± 0.05b	1.79 ± 0.1c	1.93 ± 0.03d	0.95 ± 0.07a	0.96 ± 0.09a
Fe	0.09 ± 0.01b,c	0.07 ± 0a	0.11 ± 0.02c,d	0.08 ± 0.01a,b	0.12 ± 0.02d
Mn	0.06 ± 0b,c	0.06 ± 0b	0.07 ± 0c	0.04 ± 0a	0.06 ± 0.01b,c
Cu	0.04 ± 0c	0.02 ± 0b	0.02 ± 0b	0.01 ± 0a	0.02 ± 0b
Zn	0.03 ± 0.0a	0.05 ± 0b, c	0.05 ± 0c	0.04 ± 0a, b	0.03 ± 0a

the surface, low content of polar organic functional groups and the presence of aromatic moieties (Banik et al., 2018). The easily oxidizable organic carbon (C_{oxi}) decreased with pyrolysis temperature and indicated more carbon stability of biochars obtained at high temperature.

The proximate analysis showed an increase of FC and ash and a decrease of VM with pyrolysis temperature. The low ash content in the VP and their increase in the biochars are due to the removing of volatiles in the feedstock and the accumulations of inorganic components in the ashes (Pituello et al., 2015). VM content decreased after pyrolysis at 600 °C due to dehydration of hydroxyl groups (Ronsse et al., 2013), volatilization of light compounds during pyrolysis and changes of cellulose and lignin structures (Tomczyk et al., 2020).

The N content ranged between 0.63% and 1.24% for VP and BVP300-3 h, respectively. The total C was at least 10% greater in the biochars fabricated at 600 °C than the biochars produced at 300 °C. In both pyrolysis temperatures, the carbon content increased approximately 25% in biochars compared to VP. The H content had a markedly behavior between pyrolysis temperature with the lowest values for biochars at 600 °C and the S content showed lower values for biochars compare to the biomass. The O content presented the following trend: VP > BVP300-1 h > BVP300-3 h > BVP600-3 h > BVP600-1 h. With the aforementioned results, pyrolysis temperature plays a more important role in biochars properties compared to residence time.

The highest H/C ratios were calculated for VP meanwhile the lowest was for BVP600-3 h sample. The same behavior was observed for O/C ratios. This implies that biochars had a more stable and recalcitrant carbon structure with increasing pyrolysis temperature and residence time and subsequently biochars obtained at higher temperatures are less susceptible to degradation.

As above-mentioned, the vineyard pruning waste biochars can be suitable materials as a soil ameliorant. The use of vineyard pruning waste as cover in vineyards have been tested and recommended but vineyard pruning waste derived biochars can be directly applied to soil and improve soil properties leading to relevant benefits (Egri et al., 2022). Related to this, it is important to study the biochar content of nutrients. Table 2 summarizes the total element content of VP and biochars samples. Supplementary information Table 1 provides the oxide composition of the ashes for the materials. The total P content showed differences between biochars and VP. The highest value corresponded to BVP300-1 h and with the increase of the residence time at the same temperature the total P content decreased. The total P in the biochars produced at 600 °C had lower contents than those produced at 300 °C suggesting that not all the P content was extracted for biochars at 600 °C taking to account that the P_2O_5 content remains constant in biochars at both temperatures. The K contents were similar for biochars fabricated at 300 °C and the BVP600-3 h sample. The K content for all biochars increased compared to the vineyard pruning waste, with the highest value for BVP600-1 h related to the presence of more stable forms of K (Deng et al., 2018). The oxides composition in ashes of VP and the biochars showed that K_2O also increased with pyrolysis temperature (Supplementary information Table 1). As some authors have been stated, the residence time influence was negligible at 400 °C in the K transformation process (Chen et al., 2017), the same occurred in the present work for 300 °C biochars. However, at 600 °C, the residence time influenced with the lowest K value for 3 h. The Ca content decreased for BVP300-1 h and BVP600-1 h compared to the vineyard pruning waste. However, samples BVP300-3 h and BVP600-3 h show similar Ca content than the raw material. The losses of Ca can be due to the formation of volatile compounds, which is determined by pyrolysis temperature is the determining factor. The differences with the residence time can be related to the retention of the element in surface of the char and the input of oxides (Feng et al., 2021). The percentage of CaO (Supplementary information Table 1) also increased for biochars with the highest residence time (3 h). The Na content increased for all biochars compared to vineyard pruning waste suggesting that vineyard pruning waste derived biochars can enhance the Na content and remain in the solid matrix of the material. For Na the residence time did not show any influence at 300 °C with no statistical differences between both biochars but at 600 °C the residence time of 3 h showed a higher Na value. Mg contents of biochars obtained at 300 °C were greater than for VP, with statistical differences between residence time (1 h and 3 h). At 600 °C the Mg values were lower compared to the raw material but no differences were found between 1 h and 3 h. The Fe, Mn, Cu and Zn averages were low, below 0.2 g kg^{-1} in all cases.

The highest percentages of oxides in all samples were for P_2O_5, K_2O, CaO and MgO (Supplementary information Table 1) that correspond with the high content of total P, K, Ca and Mg in the VP and biochars (Table 2). The increase of pyrolysis temperature allows the oxides to concentrate in the ashes but the changes in the residence time resulted in minor changes.

The concentration of these compounds in the biochars together with

the higher carbon content compared to the original residue demonstrates the advantages of using biochar as a soil amendment.

The FTIR spectra of the VP and derived biochars are presented in Fig. 1. The spectrum of the VP shows characteristic of lignocellulosic materials: a broad band at 3351 cm^{-1} corresponding to hydroxyl groups (Matamala et al., 2017); aliphatic C–H bonds in 2921 and 2850 cm^{-1} (Parikh et al., 2014); a peak at 1737 cm^{-1}, typical of unconjugated carboxyl (Parikh et al., 2014); peaks at 1613, 1515, 1455 and 1379 cm^{-1} assigned to aromatic skeletons of lignin (Boeriu et al., 2004); a peak at 1331 cm^{-1}, characteristic of C-O vibrations (Traoré et al., 2016); a peakband at 1158 cm^{-1}, typical of C-O asymmetric stretch in carbohydrate rings (Abdulla et al., 2010); another peak at 1062 cm^{-1}, typical of polysaccharides, resulting from C-O-C and C-OH stretches (Matamala et al., 2017; Parikh et al., 2014); the peak at 987 cm^{-1} results from C-O stretching in cellulose and lignin (Traoré et al., 2016) and finally, the peak at 839 cm^{-1} corresponds to C–H out of plane vibrations in aromatics (Niemeyer et al., 1992).

The pyrolysis produced significant changes in the spectral of biochars, altering the initial spectral lignocellulosic signature. These changes were dependent on the temperature of the pyrolysis, while the residence time had a minor effect. Heating to 300 °C produced the disappearance of peaks related to the presence of polysaccharides (those in the band between 1000 and 1150 cm^{-1}). Other changes include the decrease of the intensity of the peak at 1643 cm^{-1}, which is usually assigned to C = O carboxyl and amide I (Margenot et al., 2015), and that at 1594 cm^{-1}, related to the asymmetric carboxylic stretching (Guo and Chorover, 2003). Simultaneously, other bands become more prominent after the pyrolysis. These include the bands corresponding to OH groups (3351 and 1650 cm^{-1}), those related to C–H aliphatic groups (2921, 2850, and 1376 cm^{-1}), and that at 1422 cm^{-1}, related to aromatic C = C bonds. Increasing the pyrolysis temperature to 600 °C produced further changes in the materials. Those included the removal of peakbands in regions corresponding to OH groups (3100–3600 and 1600–1700 cm^{-1}), and those of aliphatic CH. In this case, the spectra are characterized by a broad band with peak at 1550 (aromatic C = C), 1372, 1150 and the band at 872 cm^{-1}, mostly associated with aromatic C = C, C–H (Artz et al., 2008; Ilani et al., 2005). These results are consistent with the evolution of the H/C and O/C values with the pyrolysis temperature (Table 1).

Thus, pyrolysis produced the breakdown of lignin and polysaccharides, which occur at the lowest temperature, and a progressive removal of O-containing functional groups (OH and carboxyl), which occur at different temperatures according to its nature. At 300 °C, some features from the raw material are still present, like the presence of OH and carboxylic groups. Simultaneously to the removal of O-containing functional groups, an increase in the importance of aromatic structures and C–H functional groups, and the reduction of aliphatic functional groups was observed.

Concentrations of WEOC, and UVA_{254} and $SUVA_{254}$ values of the VP and derived biochars are presented in Fig. 2, together with the EEM contour plots. The WEOC of the feedstock was 2.43 g kg^{-1}, i.e. 0.6% of the total OC. Pyrolysis produced a pronounced decrease in WEOC concentration compared to the original feedstock and this reduction was higher as pyrolysis temperature increased from 300 to 600 °C. Thus, WEOC concentrations of biochar produced by slow pyrolysis decreased exponentially as temperature increased. Residence time showed a very slight trend to affect WEOC, concentrations, which were of about 10% higher after 3 h than after 1 h; these differences can be considered as negligible. The absorbance at 254 nm (UVA_{254}) also was highest for the VP feedstock and then showed a marked decrease with pyrolysis temperature, even more pronounced than that of WEOC. However, and opposite to WEOC, UVA_{254} clearly decreased with increasing residence time. Reduction of WEOC and UVA by increased pyrolysis temperature is likely due to a higher degree of carbonization, and subsequently a decline in extractable OM.

Biochar produced at 300 °C showed higher $SUVA_{254}$, when compared to feedstock and biochar made at 600 °C, and this irrespective of residence time. This parameter is an indicator of aromaticity in the extracted solution (Weishaar et al., 2003), and also has been associated to hydrophobicity. Incomplete pyrolysis at 300 °C may result in a biochar containing more WEOC labile fraction. Therefore, decline in WEOC and raise in $SUVA_{254}$, as observed in BVP300 could result from more labile fractions in the water extract, which in turn, could increase the proportion of aromatic compounds (Fernández et al., 1997; González-Pérez et al., 2004). Remarkably, parallel results were found when heating soils at a temperature of 300 °C in aerobic conditions (Lado et al., 2023; McKay et al., 2020). The Pyrolysis at 600 °C, however, resulted in a decrease of WEOC aromaticity and hydrophobicity compared to pyrolysis at 300 °C.

The effect of residence time was similar to that of temperature; the $SUVA_{254}$ values of WEOC released by BVP300-1 h and BVP300–3 h were 0.021 and 0.014 L mg C^{-1} m^{-1}, respectively, while the corresponding values for BVP600-1 h and BVP600-3 h were 0.005 and 0.001 L mg C^{-1} m^{-1}. Thus, enlarging residence time also results in increasing WEOC aromaticity, probably as a result of a restraint in the solubilized labile fractions (Knicker, 2007; Trompowsky et al., 2005).

Fig. 2 shows EEM contours plots of VP and derived biochars. Pyrolysis changed the initial fluorescence signature, characterized by proteinaceous material, polyphenols and/or lignin, reducing the contribution of this peak, being indicative of the destruction of these

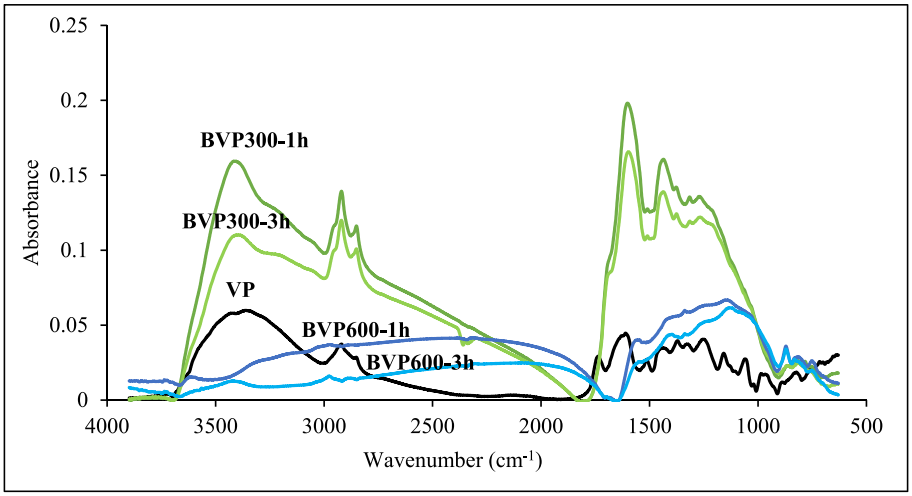

Fig. 1. FTIR spectra of VP and vineyard pruning waste derived biochars (BVP300-1 h, BVP300-3 h, BVP600-1 h and BVP600-3 h).

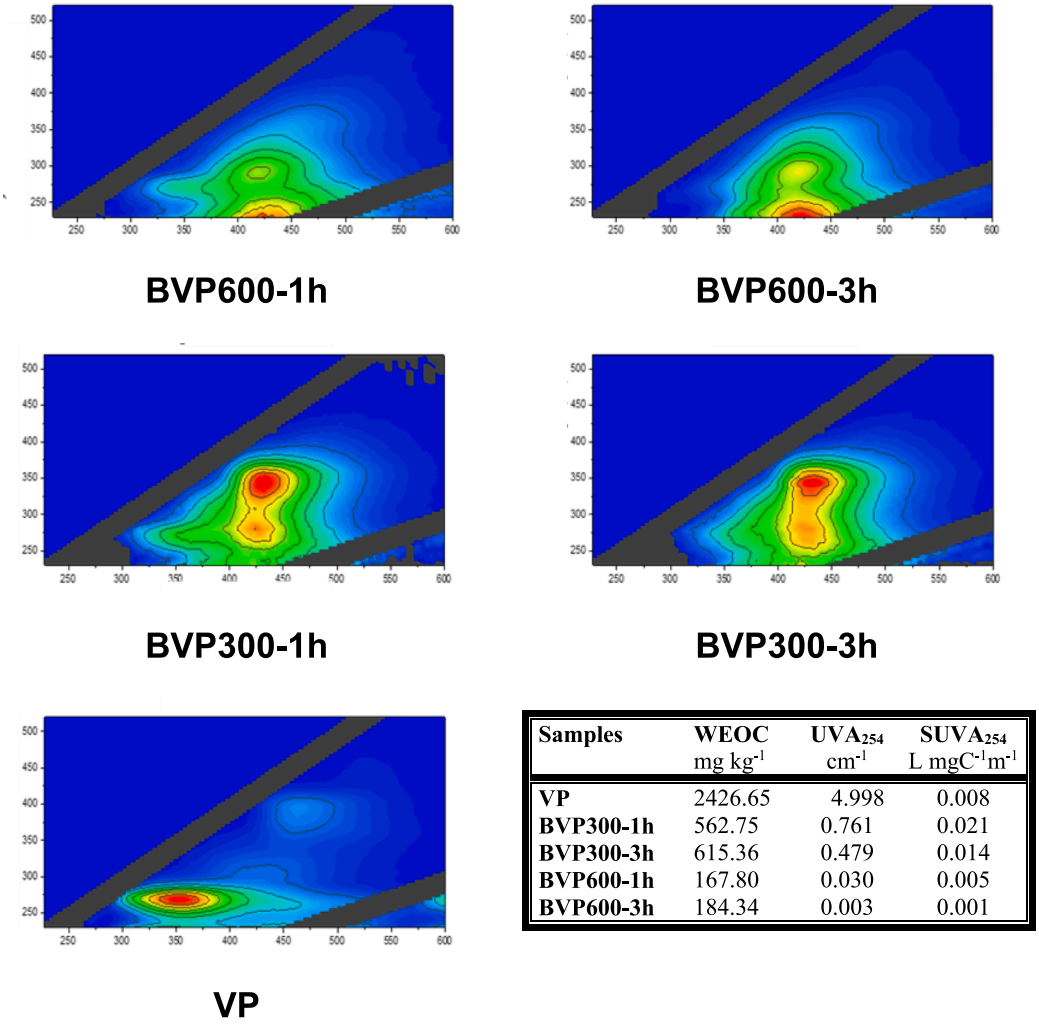

Samples	WEOC mg kg^{-1}	UVA$_{254}$ cm^{-1}	SUVA$_{254}$ L mgC^{-1}m^{-1}
VP	2426.65	4.998	0.008
BVP300-1h	562.75	0.761	0.021
BVP300-3h	615.36	0.479	0.014
BVP600-1h	167.80	0.030	0.005
BVP600-3h	184.34	0.003	0.001

Fig. 2. Fluorescence EEM contours, WEOC, UVA$_{254}$ and SUVA$_{254}$ of vineyard pruning (VP) waste and derived biochars (BVP300-1 h, BVP300-3 h, BVP600-1 h and BVP600-3 h).

compounds during pyrolysis. An increase in red-shifted emission is observed at 300 °C. It could be assumed that, the longer the emission wavelength, the higher the molecular weight of a fluorescent compound (Lichtman and Conchello, 2005) and the electronic conjugation within the aromatic system is extended over larger-size molecules. Thus, it seems that heating at 300 °C produced water-extractable compounds that are larger, more conjugated molecules than those extracted from the original vineyard pruning, with fluorescence in the region commonly attributed to humic-like components. However, a further increase in the heating temperature to 600 °C produces water-extractable compounds with fluorescence in the fulvic-like region, and therefore with peaks smaller than those characterizing the fluorescence of the 300 °C biochar extracts.

Fluorescence contour plots from biochar produced at 600 °C shows two main peaks, first a more prominent peak at λex/λem 236/420 nm, and then a second one at λex/λem 284/420 wavelengths. The former has been associated to compounds with low molecular weight, high aromaticity, and high O/C ratio, indicating a high degree of oxidation (Podgorski et al., 2018), and it has been sometimes considered fluorescence caused by fulvic-like materials (Chen et al., 2003). The latter peak has been observed in soils (Hunt and Ohno, 2007), and it has been sometimes considered caused by aliphatic compounds with low molecular weight (Lambert et al., 2016; Podgorski et al., 2018).

In relation to the effect of residence time in the fluorescence signatures, a noticeable change was a further decrease of the contribution of the fluorescence in the region of lignin/proteins when the pyrolysis duration increased from 1 to 3 h.

3.2. Physical properties

Pyrolysis of vineyard VP can produce important modifications on the physical properties, in addition to changes in the chemical composition and structure. The S_{BET} increased significantly in the biochars fabricated at 600 °C compared to S_{BET} of VP and biochars pyrolyzed at 300 °C (Supplementary information Table 2). Microspores volume was low for all the biochars and slightly increased for those obtained at 600 °C. Mesopore volumes was much higher for biochars obtained at 600 °C and also increased with residence time. The cumulative pore volume (Supplementary Information Fig. 1) clearly showed the lowest values for VP. After pyrolysis of VP, the cumulative pore volume increased specially for biochars prepared at 600 °C. In the range of pore size diameter between 0.01 and 1 μm, the samples BVP300-1 h, BVP600-1 h and BVP600-3 h showed a cumulative pore volume >2 mL g^{-1} as shown in the Supplementary information Table 2.

The hydrophysical properties of VP derived biochars are listed in Supplementary information Table 3. The BVP300-1 h showed a particular behavior compared to the other biochars with the lowest WHC and the highest AC. The BVP300-1 h presented some hydrophobicity at the moment of water saturation. The differences between the pore volume reported in Supplementary information Table 2 and the WHC could be

related to the different particle size fraction used for the respective analysis (hydrophysical properties < 4 mm and cumulative pore volume < 2 mm). Nevertheless, the values of BD, TP, WHC and AC are appropriate to consider WP derived biochars for component of growing media, except in the case of BVP300-1 h, taking into account that commercial desirable growing media had the following ranges: TP from 50 to 85%, WHC from 45 to 65% and AC from 10 to 30% and BD lower than 0.40 g cm^{-3} (Nieto et al., 2016).

Fig. 3 shows the X-ray diffraction patterns of VP and derived biochars obtained using different pyrolysis conditions. In general, XRD patterns are characterized by broad humps, which reflect the amorphous and semi- or pseudo crystalline nature of organic structures, while sharp peaks, attributed to the presence of inorganic minerals, only are observed for biochar pyrolized at 600 °C. The XRD of the VP shows humps, whose large peaks at 2θ values of 16° and 22° can be attributed to the crystalline region of cellulosic compounds in biomass (Yan et al., 2021). For biochar produced at 300 °C crystalline structure of cellulose is partially lost, although microcrystalline or amorphous cellulosic compounds may be identified. With increasing pyrolysis temperature at 600 °C these peaks are no more visible in the XRD spectra indicating that cellulose disappears by carbonization (Narzari et al., 2017).

Two broad humps in the range of 2θ = 20°-30° with a peak at about 2θ = 23° and in the range of 2θ = 38°-50° with a peak at about 2θ = 43° are observed at all XRD spectra the biochars studied. These indicate the presence of graphite aromatic layers. The former broad peak is assigned to C (200) and the latter to C (001) diffractions of graphitic and hexagonal carbons.

In the biochars pyrolized at 600 °C, a relatively sharp peak can be observed, at in the region of 2θ = 29.6 ° (Fig. 3), indicative of the presence of inorganic components, with higher crystallinity. Also, the peak intensity raises, to some degree, with increasing residence time. Notwithstanding, the amount of crystalline materials in these two biochars remains rather low. The peak position is compatible with the presence of both, calcite and rhombohedral graphite. However, calcite has been not detected neither by thermogravimetric analysis nor by FTIR spectroscopy. On the other hand, increasing temperature and residence time leads to graphitization, defined as the transformation of unordered or partially ordered non-crystalline carbon into pure carbon with an end member of crystalline graphite (Yan et al., 2021). Overall, XRD results, first show the presence of poorly crystalline graphite at the nano-size, with significantly broadened peaks. Then, at 600 °C, this nano-size material is associated with rhombohedral graphite, a less stable form than hexagonal graphite. Incomplete graphitization is most common and is expressed in the formation of carbon substances with varying degrees of structural organization (Narzari et al., 2017).

The SEM images of mature shoots (canes) and their derived biochars (Supplementary information, Fig. 2) showed regular porous structures. Cross-section micrographs (Fig. 2, A, B and C in Supplementary information) at medium resolutions (250 to 300). Pith and xylem are visible in VP and BVP300-1 h images. Limited change to the morphology of the initial feedstock can be observed as pyrolysis temperature increases. This is in accordance with previous findings (Chia et al., 2012; Suliman et al., 2016) and may be attributed to the slow pyrolysis process.

The xylem in the raw biomass (VP) is surrounded by relatively uniform parenchyma, most commonly located between vascular tissue bundles or on the outside of vascular bundles, while the biochars (BVP300-1 h and BVP600-1 h) are characterized by an open porous structure. Therefore, SEM images also suggests that the porous system of the biochar is due to the decomposition of cellulose and hemicellulose; however, lignin, having a large proportion of aromaticity, forms the visible structure in biochars. This is consistent with FTIR results.

Also average pore diameter increases with increasing temperature. The biggest pores observed in sample BVP600-1 h may result from collapse of neighboring lignin walls of neighboring xylem cells within a bundle.

The longitudinal SEM image of BVP600-1 h biochar at high-resolution (x2500) showed structures resembling graphite. These are particles in the range from about 1 to 10 μm with smooth surface, contrasting with the rougher surface of biochar particles. The presence of graphite-like particles is consistent with the presence of XRD sharp peaks attributed to rhombohedral graphite (Gorrazzi et al., 2023; Suliman et al., 2016). Incomplete graphitization and graphite-like structures are considered as indicators of long term stability.

The TG and DTA curves showed in all samples the first mass loss related to moisture content until 150 °C (Supplementary Information Fig. 3). Then the VP sample registered a significant mass loss between 200 and 400 °C related to organic matter decomposition during pyrolysis. Biochars obtained at 300 °C showed a mass loss in the same temperature range but less intense than for VP. On the contrary, biochars fabricated at 600 °C showed less mass lost in this range, but it continued at higher temperatures. This behavior during TG analysis was related to higher stability of biochars obtained at higher temperatures and their low VM content.

3.3. Environmental implications

During pyrolysis, polycyclic aromatic hydrocarbons (PAHs) can form on the surface of biochar (Bochelli et al., 2019; Greco et al., 2021), where they remain subsequently. PAHs, are thermally very stable and require high reaction energy/high temperatures to break down their

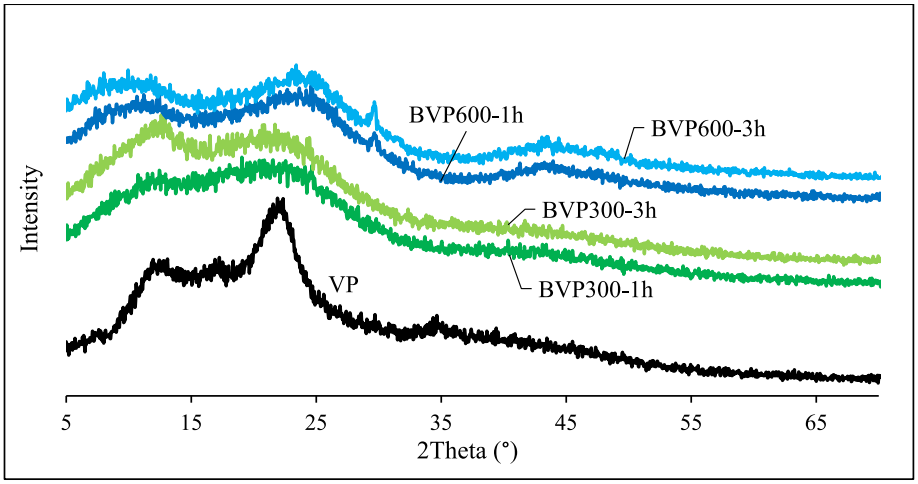

Fig. 3. X-ray diffraction analysis (XRD) for VP and vineyard pruning waste derived biochars (BVP300-1 h, BVP300-3 h, BVP600-1 h and BVP600-3 h).

chemical bonds. Sixteen out of more than thousand PAHs, have been designated High Priority Pollutants by the Environmental Protection Agency (US-EPA), because they represent the largest group of compounds that may affect human health and environmental conservation. (Santodonato et al., 1979;). Standards regulations with thresholds in water and environment for PAHs included in the 16 US-EPA list have been stablished.

In the European Biochar Certificate guidelines (EBC, 2012) PAHs concentrations in biochar were set under 4 and 12 mg kg^{-1} dry weight (dw) for premium and basic grade biochars, respectively (Schmidt et al., 2016). The International Biochar Initiative (IBI) developed the "IBI Biochar Standards, defined for safe use of biochar in soils (IBI 2015).

The PAHs concentrations of the VP derived biochars are shown in Table 3. The total PAH concentrations were higher for biochars fabricated at 300 °C compared to those produced at 600 °C. Residence time decreased PAH concentration at 300 °C and increased it at 600 °C. Following previous studies, the effect of residence time showed variable trends. For example, Wang et al. (2017), found that slow pyrolysis and longer residence time result in lower concentrations of PAHs vs fast pyrolysis. On opposite, Raclavská et al., (2018) confirmed that increased residence time resulted in a higher concentration of PAHs in the biochar.

DBA was most important accounting for the differences between biochars with 64.46 ng g^{-1} for BVP300-1 h, 33.27 ng g^{-1} for BVP300-3 h, 3.30 ng g^{-1} for BVP-600–1 h and 2.14 ng g^{-1} for BVP-600–3 h. PHEN was relatively abundant in all biochars, ranging from 23.79 to 37.56 ng g^{-1}. Light and heavy PAHs concentrations were higher in BVP300-1 h, but medium PAHs were higher in BVP600-3 h. PAHs concentrations in the derived VP biochars were lower than in other woody biochars or manure derived biochars (Greco et al., 2021; Lataf et al., 2022). Wang et al. (2017) showed total PAHs varied from < 0.1 to > 10.000 ng g^{-1}, which means 5 orders of magnitude in a logarithmic scale. Therefore, compared to other studies the PAH abundance of pruning derived biochars are in the middle range of concentrations, following the aforementioned scale. Overall, the total concentrations of 16 EPA PAHs were much lower than the threshold of 4000 ng g^{-1} stablished by the EBC for premium grade biochar.

The relatively low concentration of PAHs in VP derived biochars also is consistent with production at slow pyrolysis rates, which promote escapes to the atmosphere in gaseous form, avoiding surface capture.

The feasibility of the use of biochar as growing media component or as soil amendment also depends on its chemical and physical properties and in addition requires an assessment of the possible presence of phytotoxicity. Results of the germination index text are shown in Fig. 4. The GI for VP feedstock showed a high phytotoxicity that changed to non-phytotoxic for BVP300-1 h and BVP600-1 h. Residence time appears to have an important role, as biochars produced with larger residence time (3 h) were phytotoxic, while those produced with shorter residence time (1 h) showed no phitotoxicity; and this for both experimental temperatures. Notwithstanding, the GI values of biochars produced during prolonged residence time increased with increasing temperature; these values were 10% for VP, 40.6% for BVP300-1 h and 48.7%, for BVP300-3 h. Therefore, temperature increased GI, even if the phytotoxic effects didn't disappear at 600° C and 3 h residence time.

Germination index depends on the plant species, biochar feedstock and biochar production parameters. Until now, there are few studies analyzing phytotoxicity and results are inconclusive. For example, Benavente et al, (2018) using bochar from organic urban waste produced at 300 °C and *Lactuca sativa* as text plant, reported phytotoxic effects ranked as high for low residence time and as moderate for extended residence time. Phytotoxicity may be caused, roughly, by organic compounds contained in biochar or, in specific cases, by heavy metals or salinity (Ruzickova et al., 2021); dissolved organic compounds have been considered most responsible for phytotoxicity, including, aldehydes, ketones, carboxylic acids, PAHs, etc.

Our results didńt show a parameter robust enough to explain phytotoxicity of VP and VP derived biochars. The extreme phytotoxicity of VP may be associated with several organic compounds (either residues of chemicals applied to crop protection or water extractable composited in the pruning waste) and also with a notable concentration of Cu (40 g kg^{-1}, Table 2), More research is needed to assess phytotoxicity provenance of VP and VP derived biochars produced with extended residence time.

4. Conclusions

Our results showed that vineyard pruning waste biochars can be tailored for different environmental applications modifying pyrolysis process parameters. In particular, pyrolysis at 600 °C or 300 °C during 3 h resulted in valuable chars as a growing media component. Biochars prepared at 300 °C could improve soil fertility, whereas biochars prepared at 600 °C have a larger potential for soil carbon sequestration.

Pyrolysis at 300 or 600 °C, during 1 h, decreased the high phytotoxicity of vineyard pruning waste but a larger residence time (3 h) again resulted in phytotoxic biochars, at both temperatures.

Vineyard pruning waste can be converted into useful chars using pyrolysis as part of a valorisation strategy. Depending on the final use to be given to the pruning waste biochars, it will be necessary to optimize the temperature and pyrolysis time.

Table 3
PAHs (ng/g) of vineyard pruning waste derived biochars (BVP300-1 h, BVP300-3 h, BVP600-1 h and BVP600-3 h).

Compounds	Abbreviation	BVP300-1 h	BVP300-3 h	BVP600-1 h	BVP600-3 h
Naphthalene	NAP	0.03	0.02	0.00	0.00
Acenaphthylene	ANY	0.07	0.07	0.00	0.00
Acenaphthene	ANA	2.02	1.51	1.03	1.59
Fluorene	FLU	2.53	1.39	1.53	2.15
PAHs light	**∑ PAH light**	**4.65**	**2.99**	**2.55**	**3.75**
Phenanthrene	PHEN	24.69	23.70	24.51	37.56
Anthracene	ANT	0.91	0.48	0.56	0.92
Fluoranthene	FLT	6.89	5.95	5.17	9.12
PAHs medium	**∑ PAH medium**	**32.49**	**30.13**	**30.24**	**47.59**
Pyrene	PYR	6.31	5.37	6.09	8.70
Benz[a]anthracene	BaA	4.29	3.27	1.24	5.53
Chrysene	CHR	1.80	0.37	0.40	11.37
Benzo(b + j)fluoranthene	BbF	18.70	0.93	0.84	1.52
Benzo[k]fluoranthene	BkF	15.72	6.33	1.24	5.63
Benzo[a]pyrene	BaP	4.83	1.90	1.26	4.37
Dibenzo[a,h]anthracene	DBA	64.46	33.27	3.30	2.14
Benzo[g,h,i,]perylene	BPE	11.73	12.40	9.37	0.29
Indeno[1,2,3-cd]pyrene	IPY	9.17	10.27	9.27	0.58
PAHs heavy	**∑ PAH heavy**	**137.02**	**74.09**	**33.00**	**40.12**
PAH Total	**∑ PAH**	**174.15**	**107.21**	**65.79**	**91.46**

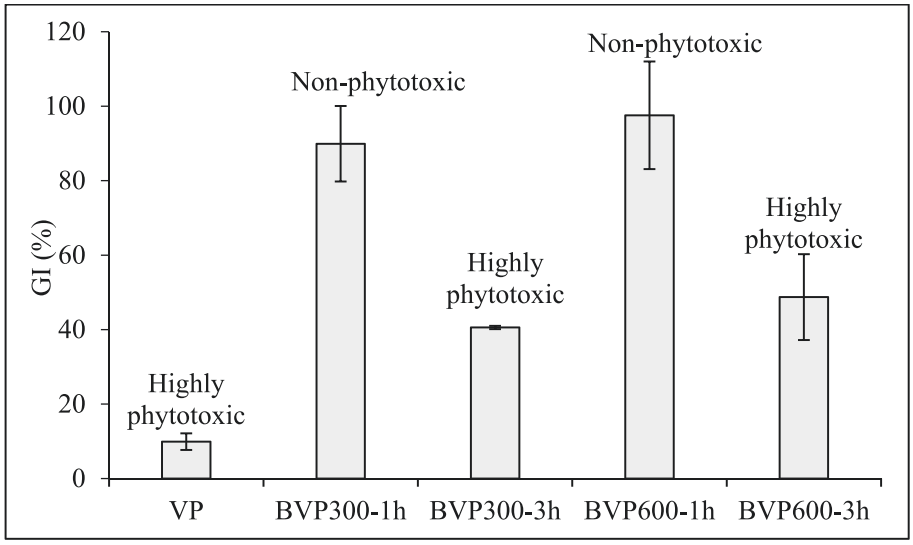

Fig. 4. Germination index for VP and vineyard pruning waste derived biochars (BVP300-1 h, BVP300-3 h, BVP600-1 h and BVP600-3 h).

5. Authors' contributions

All authors contributed to the study conceptualization and design. Analyses were performed by Eliana Cárdenas-Aguiar. The manuscript was written by all authors and all authors approved the final manuscript.

6. Funding

This work was supported by Unión Europea-NextGenerationEU [Grant number UP2021-035, 2022], Ministerio de Universidades and Universidad Politécnica de Madrid. Funding for open access charge: Universidade da Coruña/CISUG.

Declaration of Competing Interest

The authors declare that they have no known competing financial interests or personal relationships that could have appeared to influence the work reported in this paper.

Data availability

Data will be made available on request.

Appendix A. Supplementary material

Supplementary data to this article can be found online at https://doi.org/10.1016/j.wasman.2023.09.032.

References

Abdulla, H.A.N., Minor, E.C., Dias, R.F., Hatcher, P.G., 2010. Changes in the compound classes of dissolved organic matter along an estuarine transect: A study using FTIR and 13C NMR. Geochim. Cosmochim. Acta 74, 3815–3838. https://doi.org/10.1016/j.gca.2010.04.006.

Afseth, N.K., Kohler, A., 2012. Extended multiplicative signal correction in vibrational spectroscopy, a tutorial. Chemom. Intell. Lab. Syst. 117, 92–99. https://doi.org/10.1016/j.chemolab.2012.03.004.

Al-Wabel, M.I., Al-Omran, A., El-Naggar, A.H., Nadeem, M., Usman, A.R.A., 2013. Pyrolysis temperature induced changes in characteristics and chemical composition of biochar produced from conocarpus wastes. Bioresour. Technol. 131, 374–379. https://doi.org/10.1016/j.biortech.2012.12.165.

Artz, R.R.E., Chapman, S.J., Jean Robertson, A.H., Potts, J.M., Laggoun-Défarge, F., Gogo, S., Comont, L., Disnar, J.R., Francez, A.J., 2008. FTIR spectroscopy can be used as a screening tool for organic matter quality in regenerating cutover peatlands. Soil Biol. Biochem. 40, 515–527. https://doi.org/10.1016/j.soilbio.2007.09.019.

Banik, C., Lawrinenko, M., Bakshi, S., Laird, D.A., 2018. Impact of Pyrolysis Temperature and Feedstock on Surface Charge and Functional Group Chemistry of Biochars. J. Environ. Qual. 47, 452–461. https://doi.org/10.2134/jeq2017.11.0432.

Benavente, I., Gasco, G., Plaza, C., Paz-Ferreiro Choice of pyrolysis parameters for urban wastes affects soil enzymes and plant germination in a Mediterranean soil. Science of the Total Environment, Vol.634,13081314. 10.1016/j.scitotenv.2018.04.120.

Blanco-Canqui, H., 2017. Biochar and Soil Physical Properties. Soil Sci. Soc. Am. J. 81, 687–711. https://doi.org/10.2136/sssaj2017.01.0017.

Boeriu, C.G., Bravo, D., Gosselink, R.J.A., Van Dam, J.E.G., 2004. Characterisation of structure-dependent functional properties of lignin with infrared spectroscopy. Ind. Crop. Prod. 20, 205–218. https://doi.org/10.1016/j.indcrop.2004.04.022.

Borisover, M., Laor, Y., Parparov, A., Bukhanovsky, N., Lado, M., 2009. Spatial and seasonal patterns of fluorescent organic matter in Lake Kinneret (Sea of Galilee) and its catchment basin. Water Res. 43, 3104–3116. https://doi.org/10.1016/j.watres.2009.04.039.

Bucheli, T.D., Hilber, I., Schmidt, H.P., 2015. Polycyclic aromatic hydrocarbons and polychlorinated aromatic compounds in biochar. Biochar for Environmental Management: Science, Technology and Implementation 2.

Bucheli, T.D., Hilber, I., Schmidt, H., 2019. Polycyclic aromatic hydrocarbons and polychlorinated aromatic compounds in biochar. Biochar Environ. Manag. 627–656 https://doi.org/10.4324/9780203762264-28.

Cárdenas-Aguiar, E., Gascó, G., Paz-Ferreiro, J., Méndez, A., 2019. Thermogravimetric analysis and carbon stability of chars produced from slow pyrolysis and hydrothermal carbonization of manure waste. J. Anal. Appl. Pyrol. 140, 434–443. https://doi.org/10.1016/j.jaap.2019.04.026.

Chen, C., Luo, Z., Yu, C., Wang, T., Zhang, H., 2017. Transformation behavior of potassium during pyrolysis of biomass. RSC Adv. 7, 31319–31326. https://doi.org/10.1039/c7ra05162j.

Chen, W., Westerhoff, P., Leenheer, J.A., Booksh, K., 2003. Fluorescence Excitation-Emission Matrix Regional Integration to Quantify Spectra for Dissolved Organic Matter. Environ. Sci. Tech. 37, 5701–5710. https://doi.org/10.1021/es034354c.

Chia, C.H., Gong, B., Joseph, S.D., Marjo, C.E., Munroe, P., Rich, A.M., 2012. Imaging of mineral-enriched biochar by FTIR, Raman and SEM-EDX. Vib. Spectrosc 62, 248–257. https://doi.org/10.1016/j.vibspec.2012.06.006.

Ciesielski, H., Sterckeman, T., 1997. Determination of cation exchange capacity and exchangeable cations in soils by means of cobalt hexamine trichloride. Effets of experimental conditions. Agron. Agric. Environ. 17, 1–7.

Deng, L., Ye, J., Jin, X., Che, D., 2018. Transformation and release of potassium during fixed-bed pyrolysis of biomass. J. Energy Inst. 91, 630–637. https://doi.org/10.1016/j.joei.2017.02.009.

Devi, P., Saroha, A.K., 2015. Effect of pyrolysis temperature on polycyclic aromatic hydrocarbons toxicity and sorption behaviour of biochars prepared by pyrolysis of paper mill effluent treatment plant sludge. Bioresour. Technol. 192, 312–320. https://doi.org/10.1016/j.biortech.2015.05.084.

EBC, 2012. European Biochar Certificate - Guidelines for a Sustainable Production of Biochar'. Eur. Biochar Found. (EBC), Arbaz, Switzerland. 10.13140/RG.2.1.4658.7043. Version 9.0E 1st June. (2020) 1–22.

Egri, D., Pârvulescu, O.C., Ion, V.A., Răducanu, C.E., Calcan, S.I., Bădulescu, L., Madjar, R., Orbeci, C., Dobre, T., Moț, A., Iliescu, L.M., Crăciun, M.E., 2022. Vine Pruning-Derived Biochar for Agronomic Benefits. Agronomy 12, 1–15. https://doi.org/10.3390/agronomy12112730.

Feng, Z., Pang, K., Bai, Z., Hou, R., Ye, D., Guo, Z., Kong, L., Bai, J., Li, W., 2021. Occurrence and transformation of sodium and calcium species in mild liquefaction solid product of Hami coal during pyrolysis. Fuel 286, 119489. https://doi.org/10.1016/j.fuel.2020.119489.

Feng, D., Wang, S., Zhang, Y., Zhao, Y., Sun, S., Chang, G., Lai, X., Tan, H., Qin, Y., 2020. Review of Carbon Fixation Evaluation and Emission Reduction Effectiveness for Biochar in China. Energy Fuel 34, 10583–10606. https://doi.org/10.1021/acs.energyfuels.0c02396.

Fernández, I., Cabaneiro, A., Carballas, T., 1997. Organic matter changes immediately after a wildfire in an atlantic forest soil and comparison with laboratory soil heating. Soil Biol. Biochem. 29, 1–11. https://doi.org/10.1016/S0038-0717(96)00289-1.
Florindo, T., Ferraz, A.I., Rodrigues, A.C., Nunes, L.J.R., 2022. Residual Biomass Recovery in the Wine Sector: Creation of Value Chains for Vine Pruning. Agric. 12, 1–18. https://doi.org/10.3390/agriculture12050670.
Gascó, G., Paz-Ferreiro, J., Álvarez, M.L., Saa, A., Méndez, A., 2018. Biochars and hydrochars prepared by pyrolysis and hydrothermal carbonisation of pig manure. Waste Manag. 79, 395–403. https://doi.org/10.1016/j.wasman.2018.08.015.
Głąb, T., Palmowska, J., Zaleski, T., Gondek, K., 2016. Effect of biochar application on soil hydrological properties and physical quality of sandy soil. Geoderma 281, 11–20. https://doi.org/10.1016/j.geoderma.2016.06.028.
González-Pérez, J.A., González-Vila, F.J., Almendros, G., Knicker, H., 2004. The effect of fire on soil organic matter - A review. Environ. Int. 30, 855–870. https://doi.org/10.1016/j.envint.2004.02.003.
Gorrazzi, S.A., Massazza, D., Pedetta, A., Silva, L., Prados, B., Fouga, G., Bonanni, S., 2023. Biochar as a substitute for graphite in microbial electrochemical technologies. RSC Sustain. 1200–1210 https://doi.org/10.1039/d3su00041a.
Greco, G., Videgain, M., Di Stasi, C., Pires, E., Manyà, J.J., 2021. Importance of pyrolysis temperature and pressure in the concentration of polycyclic aromatic hydrocarbons in wood waste-derived biochars. J. Anal. Appl. Pyrol. 159 https://doi.org/10.1016/j.jaap.2021.105337.
Guo, M., Chorover, J., 2003. Transport and fractionation of dissolved organic matter in soil columns. Soil Sci. 168, 108–118. https://doi.org/10.1097/00010694-200302000-00005.
Holbrook, R.D., Derose, P.C., Leigh, S.D., Rukhin, A.L., Heckert, N.A., 2006. Excitation-emission matrix fluorescence spectroscopy for natural organic matter characterization: A quantitative evaluation of calibration and spectral correction procedures. Appl. Spectrosc. 60, 791–799. https://doi.org/10.1366/000370206777886973.
Hunt, J.F., Ohno, T., 2007. Characterization of fresh and decomposed dissolved organic matter using excitation-emission matrix fluorescence spectroscopy and multiway analysis. J. Agric. Food Chem. 55, 2121–2128. https://doi.org/10.1021/jf063336m.
Igalavithana, A.D., Mandal, S., Niazi, N.K., Vithanage, M., Parikh, S.J., Mukome, F.N.D., Rizwan, M., Oleszczuk, P., Al-Wabel, M., Bolan, N., Tsang, D.C.W., Kim, K.H., Ok, Y. S., 2017. Advances and future directions of biochar characterization methods and applications. Crit. Rev. Environ. Sci. Technol. 47, 2275–2330. https://doi.org/10.1080/10643389.2017.1421844.
Ilani, T., Schulz, E., Chefetz, B., 2005. Interactions of Organic Compounds with Wastewater Dissolved Organic Matter: Role of Hydrophobic Fractions. J. Environ. Qual. 34, 552–562. https://doi.org/10.2134/jeq2005.0552.
International Biochar Initiative, 2015. Standardized Product Definition and Product Testing Guidelines for Biochar That Is Used in Soil. Int. Biochar Initiat. https://doi.org/10.1016/j.zefq.2013.07.002.
Knicker, H., 2007. How does fire affect the nature and stability of soil organic nitrogen and carbon? A review. Biogeochemistry 85, 91–118. https://doi.org/10.1007/s10533-007-9104-4.
Kothawala, D.N., Murphy, K.R., Stedmon, C.A., Weyhenmeyer, G.A., Tranvik, L.J., 2013. Inner filter correction of dissolved organic matter fluorescence. Limnol. Oceanogr. Methods 11, 616–630. https://doi.org/10.4319/lom.2013.11.616.
Lado, M., Sayegh, J., Gia Gadňay, A., Ben-Hur, M., Borisover, M., 2023. Heat-induced changes in soil water-extractable organic matter characterized using fluorescence and FTIR spectroscopies coupled with dimensionality reduction methods. Geoderma 430. https://doi.org/10.1016/j.geoderma.2023.116347.
Lakowicz, J.R., 2013. Principles of Fluorescence Spectroscopy, Third. ed, Springer science & business media. Baltimore. 10.1007/978-1-4615-7658-7_10.
Lambert, T., Bouillon, S., Darchambeau, F., Massicotte, P., Borges, A.V., 2016. Shift in the chemical composition of dissolved organic matter in the Congo River network. Biogeosciences 13, 5405–5420. https://doi.org/10.5194/bg-13-5405-2016.
Lataf, A., Jozefczak, M., Vandecasteele, B., Viaene, J., Schreurs, S., Carleer, R., Yperman, J., Marchal, W., Cuypers, A., Vandamme, D., 2022. The effect of pyrolysis temperature and feedstock on biochar agronomic properties. J. Anal. Appl. Pyrol. 168, 105728 https://doi.org/10.1016/j.jaap.2022.105728.
Lehmann, J., Rillig, M.C., Thies, J., Masiello, C. a., Hockaday, W.C., Crowley, D., 2011. Biochar effects on soil biota - A review. Soil Biol. Biochem. 43, 1812–1836. 10.1016/j.soilbio.2011.04.022.
Lichtman, J.W., Conchello, J.A., 2005. Fluorescence microscopy. Nat. Methods 2, 910–919. https://doi.org/10.1038/nmeth817.
Liland, K.H., 2021. EMSC: Extended Multiplicative Signal Correction. R Packag. version (9), 3.
Liu, Y., Wang, L., Wang, X., Jing, F., Chang, R., Chen, J., 2020. Oxidative ageing of biochar and hydrochar alleviating competitive sorption of Cd(II) and Cu(II). Sci. Total Environ. 725, 138419 https://doi.org/10.1016/j.scitotenv.2020.138419.
Mandal, S., Donner, E., Vasileiadis, S., Skinner, W., Smith, E., Lombi, E., 2018. The effect of biochar feedstock, pyrolysis temperature, and application rate on the reduction of ammonia volatilisation from biochar-amended soil. Sci. Total Environ. 627, 942–950. https://doi.org/10.1016/j.scitotenv.2018.01.312.
Margenot, A.J., Calderón, F.J., Bowles, T.M., Parikh, S.J., Jackson, L.E., 2015. Soil Organic Matter Functional Group Composition in Relation to Organic Carbon, Nitrogen, and Phosphorus Fractions in Organically Managed Tomato Fields. Soil Sci. Soc. Am. J. 79, 772–782. https://doi.org/10.2136/sssaj2015.02.0070.
Matamala, R., Calderón, F.J., Jastrow, J.D., Fan, Z., Hofmann, S.M., Michaelson, G.J., Mishra, U., Ping, C.L., 2017. Influence of site and soil properties on the DRIFT spectra of northern cold-region soils. Geoderma 305, 80–91. https://doi.org/10.1016/j.geoderma.2017.05.014.
McKay, G., Hohner, A.K., Rosario-Ortiz, F.L., 2020. Use of optical properties for evaluating the presence of pyrogenic organic matter in thermally altered soil leachates. Environ. Sci. Process. Impacts 22, 981–992. https://doi.org/10.1039/c9em00413k.
Méndez, A., Paz-Ferreiro, J., Gil, E., Gascó, G., 2015. The effect of paper sludge and biochar addition on brown peat and coir based growing media properties. Sci. Hortic. (Amsterdam) 193, 225–230. https://doi.org/10.1016/j.scienta.2015.07.032.
Narzari, R., Bordoloi, N., Sarma, B., Gogoi, L., Gogoi, N., Borkotoki, B., Kataki, R., 2017. Fabrication of biochars obtained from valorization of biowaste and evaluation of its physicochemical properties. Bioresour. Technol. 242, 324–328. https://doi.org/10.1016/j.biortech.2017.04.050.
Nelson, D.W., Sommers, L.E., 1996. Total Carbon , Organic Carbon , and Organic Matter, in: Soil Science Society of America and American Society of Agronomy (Ed.), Methods of Soil Analysis Part 3—Chemical Methods. pp. 961–1009.
Niemeyer, J., Chen, Y., Bollag, J.-M., 1992. Characterization of Humic Acids, Composts, and Peat by Diffuse Reflectance Fourier-Transform Infrared Spectroscopy. Soil Sci. Soc. Am. J. 56, 135–140. https://doi.org/10.2136/sssaj1992.03615995005600010021x.
Nieto, A., Gascó, G., Paz-Ferreiro, J., Fernández, J.M., Plaza, C., Méndez, A., 2016. The effect of pruning waste and biochar addition on brown peat based growing media properties. Sci. Hortic. (Amsterdam) 199, 142–148. https://doi.org/10.1016/j.scienta.2015.12.012.
Obia, A., Mulder, J., Martinsen, V., Cornelissen, G., Børresen, T., 2016. In situ effects of biochar on aggregation, water retention and porosity in light-textured tropical soils. Soil Tillage Res. 155, 35–44. https://doi.org/10.1016/j.still.2015.08.002.
Parikh, S.J., Goyne, K.W., Margenot, A.J., Mukome, F.N.D., Calderón, F.J., 2014. Chapter One -Soil chemical insights provided through vibrational spectroscopy. In: Sparks, D. L. (Ed.), Advances in Agronomy. Academic Press, pp. 1–148. https://doi.org/10.1016/B978-0-12-800132-5.00001-8.
Pituello, C., Francioso, O., Simonetti, G., Pisi, A., Torreggiani, A., Berti, A., Morari, F., 2015. Characterization of chemical–physical, structural and morphological properties of biochars from biowastes produced at different temperatures. J. Soil. Sediment. 15, 792–804. https://doi.org/10.1007/s11368-014-0964-7.
Podgorski, D.C., Zito, P., McGuire, J.T., Martinovic-Weigelt, D., Cozzarelli, I.M., Bekins, B.A., Spencer, R.G.M., 2018. Examining Natural Attenuation and Acute Toxicity of Petroleum-Derived Dissolved Organic Matter with Optical Spectroscopy. Environ. Sci. Tech. 52, 6157–6166. https://doi.org/10.1021/acs.est.8b00016.
Raclavská, H., Růžičková, J., Škrobánková, H., Koval, S., Kucbel, M., Raclavský, K., Švédová, B., Pavlík, P., Juchelková, D., 2018. Possibilities of the utilization of char from the pyrolysis of tetrapak. J. Environ. Manage. 219, 231–238. https://doi.org/10.1016/j.jenvman.2018.05.002.
Razzaghi, F., Obour, P.B., Arthur, E., 2020. Does biochar improve soil water retention? A systematic review and meta-analysis. Geoderma 361, 114055. https://doi.org/10.1016/j.geoderma.2019.114055.
Ronsse, F., van Hecke, S., Dickinson, D., Prins, W., 2013. Production and characterization of slow pyrolysis biochar: Influence of feedstock type and pyrolysis conditions. GCB Bioenergy 5, 104–115. https://doi.org/10.1111/gcbb.12018.
Santodonato, J., Howard, P., Basu, D., Lande, S., Selkirk, J., 1979. Health assessment document for polycyclic organic matter. Final report.
Schmidt, H.P., Bucheli, T.D., Kammann, C., Glaser, B., Abiven, S., Leifeld, J., 2016. European Biochar Certificate - Guidelines for a sustainable production of Biochar. Eur. Biochar Found. (EBC). 1–22. 10.13140/RG.2.1.4658.7043.
Ruzickova, J., Koval, S., Raclavska, H., Kucbel, M., Svedova, B., Raclavsky, K., Scala, F., 2021. A comprehensive assessment of potential hazard caused by organic compounds in biochar for agricultural use. Journal of hazardous materials 403, 123644.
Suliman, W., Harsh, J.B., Abu-Lail, N.I., Fortuna, A.M., Dallmeyer, I., Garcia-Perez, M., 2016. Influence of feedstock source and pyrolysis temperature on biochar bulk and surface properties. Biomass Bioenergy 84, 37–48. https://doi.org/10.1016/j.biombioe.2015.11.010.
Tomczyk, A., Sokołowska, Z., Boguta, P., 2020. Biochar physicochemical properties: pyrolysis temperature and feedstock kind effects. Rev. Environ. Sci. Biotechnol. 19, 191–215. https://doi.org/10.1007/s11157-020-09523-3.
Traoré, M., Kaal, J., Martínez Cortizas, A., 2016. Application of FTIR spectroscopy to the characterization of archeological wood. Spectrochim. Acta - Part A Mol. Biomol. Spectrosc. 153, 63–70. https://doi.org/10.1016/j.saa.2015.07.108.
Trompowsky, P.M., De Melo Benites, V., Madari, B.E., Pimenta, A.S., Hockaday, W.C., Hatcher, P.G., 2005. Characterization of humic like substances obtained by chemical oxidation of eucalyptus charcoal. Org Geochem. 36, 1480–1489. https://doi.org/10.1016/j.orggeochem.2005.08.001.
U.S. EPA. 2007. "Method 3051A (SW-846): Microwave Assisted Acid Digestion of Sediments, Sludges, and Oils," Revision 1. Washington, DC.
Wang, C., Wang, Y., Herath, H.M.S.K., 2017. Polycyclic aromatic hydrocarbons (PAHs) in biochar – Their formation, occurrence and analysis: A review. Org Geochem. 114, 1–11. https://doi.org/10.1016/j.orggeochem.2017.09.001.
Wang, S., Zhang, H., Haiyan Huang, H., Xiao, R., Li, R., Zhang, Z., 2020. Influence of temperature and characteristics of biochars derived from agricultural residues: A comprehensive evaluation. Process Saf. Environ. Prot. 139, 218–229. https://doi.org/10.1016/j.psep.2020.03.028.
Weishaar, J.L., Aiken, G.R., Bergamaschi, B.A., Fram, M.S., Fujii, R., Mopper, K., 2003. Evaluation of specific ultraviolet absorbance as an indicator of the chemical composition and reactivity of dissolved organic carbon. Environ. Sci. Tech. 37, 4702–4708. https://doi.org/10.1021/es030360.

Wong, J.W.C., Ogbonnaya, U.O., 2021. Biochar porosity : a nature-based dependent parameter to deliver microorganisms to soils for land restoration. Environ. Sci. Pollut. Res. 28, 46894–46909. https://doi.org/10.1007/s11356-021-14803-8.
Yan, Y., Manickam, S., Lester, E., Wu, T., Pang, C.H., 2021. Synthesis of graphene oxide and graphene quantum dots from miscanthus via ultrasound-assisted mechano-chemical cracking method. Ultrason. Sonochem. 73, 105519 https://doi.org/10.1016/j.ultsonch.2021.105519.
Zucconi, F., Monaco, A., Forte, M., Bertoldi, M. de., 1985. Phytotoxins during the stabilization of organic matter. Compost. Agric. other wastes / Ed. by J.K.R. Gasser.

Further reading

Channiwala, S.A., Parikh, P.P., 2002. A unified correlation for estimating HHV of solid, liquid and gaseous fuels. Fuel 81, 1051–1063. https://doi.org/10.1016/S0016-2361(01)00131-4.